Applied Physics A (2018) 124:411
https://doi.org/10.1007/s00339-018-1824-x

Applied Physics A
Materials Science & Processing

Titanium nitride formation by a dual-stage femtosecond laser process

S. Hammouti[1] · B. Holybee[1] · W. Zhu[1] · J. P. Allain[1] · B. Jurczyk[2] · D. N. Ruzic[1]

Received: 31 January 2018 / Accepted: 25 April 2018 / Published online: 8 May 2018

Abstract
Formation of TiN by femtosecond laser processing in controlled gas atmosphere is reported. A dual-stage process was designed and aimed to first remove and restructure the native oxide layer of titanium surface through laser irradiation under an argon-controlled atmosphere, and then to maximize titanium nitride formation through an irradiation under a nitrogen reactive environment. An extensive XPS study was performed to identify and quantify laser-induced titanium surface chemistry modifications after a single-stage laser process (Ar and N_2 individually), and a dual-stage laser process. The importance of each step that composes the dual-stage laser process was demonstrated and leads to the dual-stage laser process for the formation of TiO, Ti_2O_3 and TiN. In this study, the largest nitride formation occurs for the dual stage process with laser conditions at 4 W/1.3 J cm^{-2} under argon and 5 W/1.6 J cm^{-2} under nitrogen, yielding a total TiN composition of 8.9%. Characterization of both single-stage and dual-stage laser process-induced surface morphologies has been performed as well, leading to the observation of a wide range of hierarchical surface structures such as high-frequency ripples, grooves, protuberances and pillow-like patterns. Finally, water wettability was assessed by means of contact angle measurements on untreated titanium surface, and titanium surfaces resulting from either single-stage laser process or dual-stage laser process. Dual-stage laser process allows a transition of titanium surface, from phobic (93°) to philic (35°), making accessible both hydrophilic and chemically functionalized hierarchical surfaces.

1 Introduction

These last decades, surface functionalization by femtosecond laser was extensively investigated on a wide range of material due to the collaborative effects of the topography and surface chemistry induced by this type of process [1–4]. Laser parameters such as beam diameter, number of pulses, repetition rate, fluence or orientation of the polarization have a great influence on the surface properties [5–7]. Wide variety of self-organized surface structures (spikes, pores, ripples or laser induced periodic surface structures) generated by ultra-short pulses irradiation [8–10], as well as controlled laser surface texturing (dimple patterns geometrically controlled) are attractive for specific related surface applications such as tribology or biomedical [11–13]. Nevertheless, if the application requires surface chemistry modifications, laser surface treatment may be limited by oxidation phenomenon when processed in air. This can be addressed by performing laser treatment in a closed enclosure with a reactive atmosphere. Direct laser synthesis in a reactive gas environment is an alternative technique that allows the formation of a coating layer by chemically modifying the surface itself contrary to classical manufacturing processes such as PVD or CVD. High mechanical performance coatings such as TiN largely used in aeronautic components or medical implants can be produced by performing laser irradiation in a nitrogen atmosphere and is called laser nitriding [14]. Laser nitriding of titanium has already been demonstrated as an efficient way to form TiN for a wide range of laser such as free electron, excimer, nanosecond and femtosecond [15–17]. Nevertheless, native oxide layer remains an obstacle to form TiN compound. Therefore, a two-stage femtosecond laser process was designed and includes consecutively an argon-controlled atmosphere laser process stage and a nitrogen-controlled atmosphere laser process stage. The argon atmosphere stage intends to both remove and restructure the native oxide layer of titanium, while the nitrogen atmosphere stage

S. Hammouti and B. Holybee are first authors of this paper.

✉ D. N. Ruzic
druzic@illinois.edu

[1] Center for Plasma-Material Interactions, University of Illinois at Urbana Champaign, 201 S Goodwin Avenue, Urbana, IL 61801, USA

[2] Starfire Industries, LLC, 2109 S Oak St, Champaign, IL 61820, USA

aims to maximize titanium nitride formation. Detailed XPS and topographic studies using SEM and AFM are performed to quantify effects induced by both individual laser process stage (Ar or N_2) and dual stage laser process. Surface properties of fs laser-treated titanium are then explored by contact angles measurements.

2 Experimental section

2.1 Femtosecond laser surface processing in a reactive environment

A Coherent Monaco femtosecond diode pumped laser system with linearly polarized light was used for the laser processing of titanium samples surfaces. This laser operates at a central wavelength of 1040 nm (Full Width at Half Maximum), pulse length 350 fs, at a maximum power of 40 W when repetition rate is set at 1 MHz. A dual axis galvanometer system (GVS012(/M), Thorlabs) and a F-Theta lens (FTH160-1064, Thorlabs) were used to focus and steer the beam over the surface. The maximum field size is 110 × 110 mm with a repeatability of 5 µm. A schematic representation of the setup developed to perform 2D laser surface texturing is shown in Fig. 1. Software was developed under LabVIEW to control the pattern of the texturing based on an imported image. Dimension of the texturing in both *X* and *Y* axis is related to the number of pixels which compose the image while the number of pulses delivered per spot is proportional to the value of each pixel. For this purpose, both galvometer's drivers that control the rotation of mirrors are connected to a 9269 NI DAQ card and the gate of the laser system is connected to a 9401 NI digital module. The peak fluence was calculated from Eq. 1, assuming a Gaussian beam shape [18]:

$$F = \frac{2P}{f\pi\left(\omega_0/2\right)^2}\ [\mathrm{J\ cm^{-2}}] \tag{1}$$

where P is the laser power, f the repetition rate and ω_0 the radius of the beam spot at $1/e^2$. Repetition rate f remained unchanged for all laser treatments and set at 1 MHz. ω_0 (defined at $1/e^2$ of peak intensity) was assessed by the

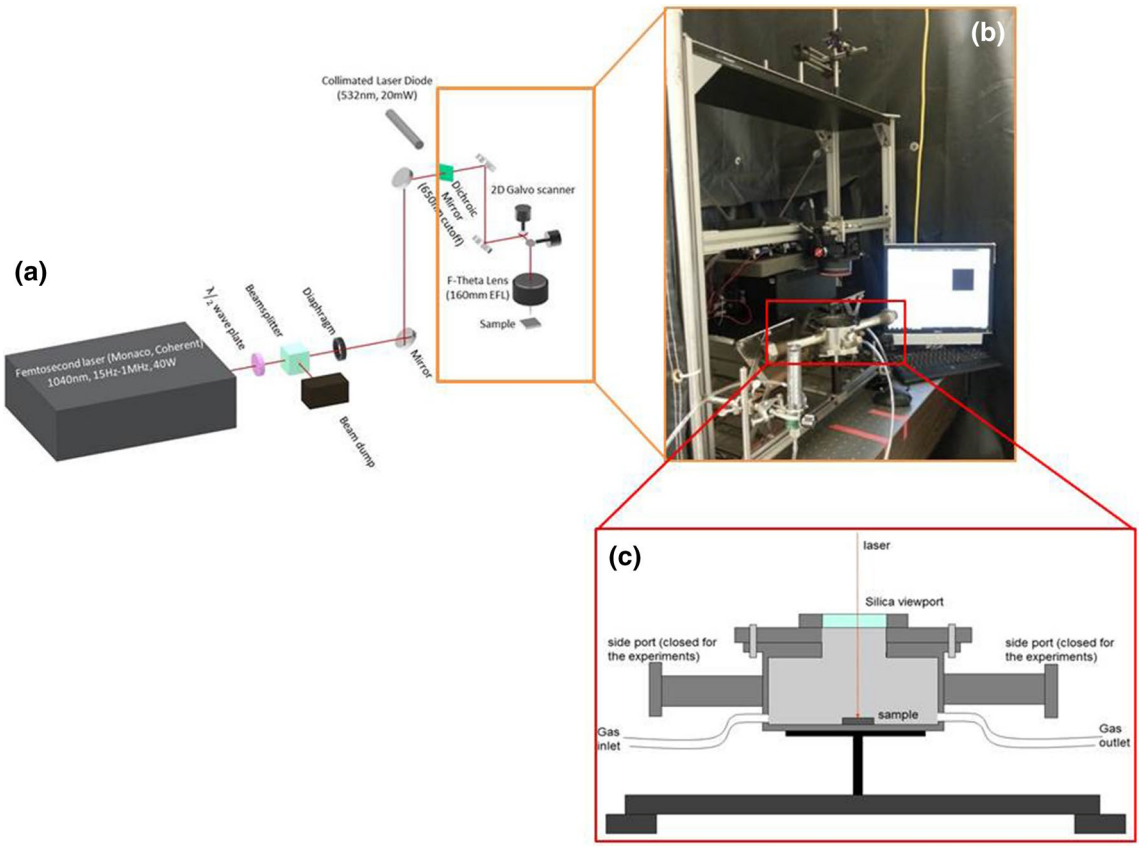

Fig. 1 **a** Schematic showing the experimental setup for the controlled atmosphere laser processing experiments. **b** Photo of the workstation during dual-stage laser process experiments. **c** Schematic section of the vacuum chamber including fs laser-treated titanium sample under controlled atmosphere (Ar or N_2)

technique developed and described by Liu [19]. It consists of analyzing series of laser impacts made by varying the energy of the beam and then determining the size of the beam from the size of the impacts obtained in the ablative regime. The spot size was found to be 40 ± 2.3 µm. A cylindrical vacuum chamber (Kurt J. Lesker) was used to perform the laser surface texturing in a reactive gas atmosphere. According to the step of the laser treatment, an argon cylinder or a nitrogen cylinder was connected to the gas inlet of the chamber. To control atmosphere conditions, a constant flow of gas (Ar or N_2), with a flow rate set at 2.5 L/min (Flowmeter for inert gas, Mc Master-Carr) filled the chamber during laser processing experiments. A high vacuum viewport (High Vacuum ConFlat Viewport, Thorlabs) with a 38.1 mm diameter fused silica window was sealed on the top of the chamber to allow the transmission of the infrared laser beam. Laser power was measured and set to the desired value before each surface laser processing by means of a high damage threshold power detector (Gentec-EO, UP19K, 50 W) just after the F-theta lens. Titanium plates with initial dimensions of 1 mm × 76 mm × 76 mm (99.6%, grade 2, Solutions materials, LLC) have been cut to titanium sheets of 1 mm × 15 mm × 15 mm dimensions and used for both single and dual stage laser process experiments. No polishing has been performed prior to laser processing.

Areas of 5 mm × 1 mm were processed by laser on titanium surfaces either through a single-stage laser process or the dual-stage laser process, with Fig. 2 showing the titanium sample with laser tracks after dual-stage laser processing experiments. During the dual-stage laser process experiments, laser texturing on the titanium surface was overlapped by keeping the start position of the beam constant on the sample surface. Tables 1 and 2 present laser parameters used for single-stage laser process experiments and dual-stage laser process experiments. In both tables, cumulative power density ${}^{N}P_{D}$ parameter has been calculated following Eq. 2 [20]:

$$ {}^{N}P_{D} = \frac{F}{\tau_{p}} N \ (\mathrm{W\ cm^{-2}}) \tag{2} $$

where τ_p is the pulse width (350 fs at FWHM). Cumulative power density is a parameter that is particularly relevant for assessing the contribution of the number of pulses per spot N, as well as the fluence F of each performed laser treatment and facilitates comparison. In total, five titanium samples referred as 0_1_X, 0_2_X, 1_X (Fig. 2a), 2_X and 3_X (with X the type of laser treatment applied according to Tables 1, 2) have been investigated.

Table 1 Laser parameters used for single-stage laser process experiments: laser irradiation under argon atmosphere only (samples referred 0_1_X), and laser irradiation under nitrogen atmosphere only (samples referred 0_2_X)

Ref. sample	Reactive gas	N	P (W)	F (J cm^{-2})	${}^{N}P_{D}$ (W cm^{-2})
0_1_1	Argon	10,000	3	0.95	2.7E+16
0_1_2	Argon	10,000	3.5	1.1	3.2E+16
0_1_3	Argon	10,000	4	1.3	3.6E+16
0_2_1	Nitrogen	10,000	3.5	1.1	3.2E+16
0_2_2	Nitrogen	10,000	4	1.3	3.6E+16
0_2_3	Nitrogen	10,000	4.5	1.4	4.1E+16
0_2_4	Nitrogen	10,000	5	1.6	4.5E+16

2.2 Topography characterization

The observations of surface morphologies after laser irradiation were performed by scanning electron microscopy (SEM, JEOL 7000 and Hitachi S-4700) and atomic force

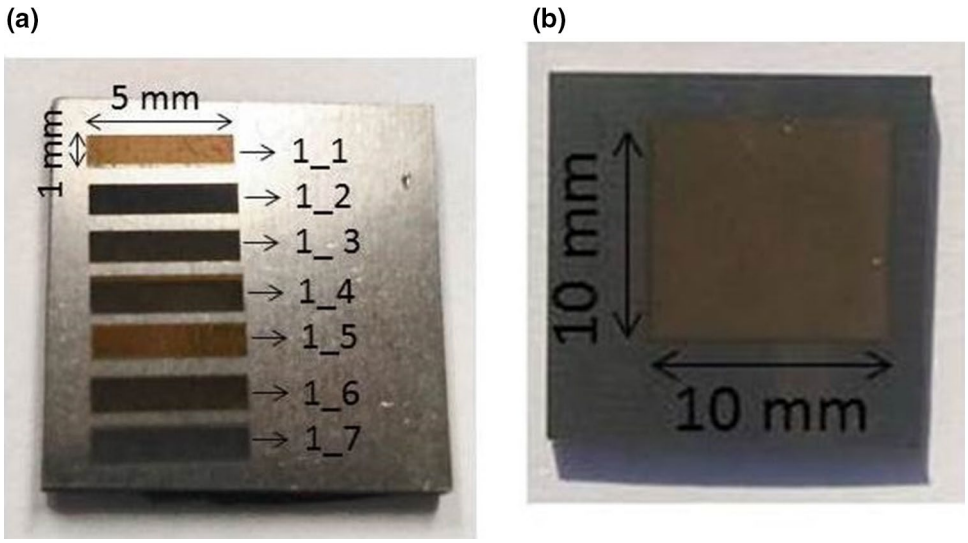

Fig. 2 Photo of the 15 mm × 15 mm titanium sample referred 1_X, which exhibits seven test areas of 1 mm × 5 mm dimensions performed by means of dual-stage laser process experiments (**a**). Photo of 10 mm × 10 mm area subjected to dual-stage laser process at Ar: 4 W/1.3 J cm^{-2} and N_2: 5 W/1.6 J cm^{-2} (10,000 pulses), and used for water wettability assessment (**b**)

Table 2 Laser Parameters used for dual-stage laser process experiments: laser pretreatment under argon atmosphere followed by a laser irradiation under nitrogen atmosphere (samples referred 1_X, 2_X and 3_X)

Ref. sample	Gas environment	N	P (W)	F (J cm^{-2})	$^{N}P_{D}$ (W cm^{-2})
1_1	Argon	10,000	3	0.95	2.7E+16
	Nitrogen	10,000	4	1.3	3.6E+16
1_2	Argon	10,000	4	1.3	3.6E+16
	Nitrogen	10,000	4	1.3	3.6E+16
1_3	Argon	10,000	3.5	1.1	3.2E+16
	Nitrogen	10,000	4	1.3	3.6E+16
1_4	Argon	10,000	4	1.3	3.6E+16
	Nitrogen	10,000	5	1.6	4.5E+16
1_5	Argon	10,000	3	0.95	2.7E+16
	Nitrogen	10,000	5	1.6	4.5E+16
1_6	Argon	10,000	4	1.3	3.6E+16
	Nitrogen	10,000	4.5	1.4	4.1E+16
1_7	Argon	10,000	4	1.3	3.6E+16
	Nitrogen	10,000	3.5	1.1	3.2E+16
2_2	Argon	15,000	3	0.95	4.1E+16
	Nitrogen	10,000	5	1.6	4.5E+16
2_3	Argon	1000	7	2.2	6.4E+15
	Nitrogen	10,000	5	1.6	4.5E+16
2_4	Argon	5000	7	2.2	3.2E+16
	Nitrogen	10,000	5	1.6	4.5E+16
2_5	Argon	3000	6	1.9	1.6E+16
	Nitrogen	10,000	6	1.9	5.4E+16
3_1	Argon	10,000	5	1.6	4.5E+16
	Nitrogen	10,000	6	1.9	5.4E+16
3_2	Argon	10,000	6	1.9	5.4E+16
	Nitrogen	10,000	7	2.2	6.4E+16

microscopy (AFM, Asylum Cypher) in tapping mode when the topography scale allowed it, as it is the case for laser-induced self-organized nanostructures. Gwyddion software was used to visualize and investigate 3D AFM scans [21].

2.3 X-ray photoelectron spectroscopy (XPS)

To investigate the surface chemistry induced by the femtosecond laser, XPS measurements were made after the samples were exposed to air (ex-situ) using a Kratos Axis Ultra X-ray photoelectron spectrometer (Kratos Analytical, Inc., Manchester, UK) using monochromatic Al Kα radiation (1486.6 eV). High-resolution spectra were collected at a take-off angle of 90° using a pass energy of 40 eV from a 0.7 mm × 0.3 mm area using the hybrid (electrostatic and magnetic immersion) lens mode. The samples were affixed onto the sample holder using double-sided copper tape. The binding energy scale was referenced and calibrated to the adventitious C 1 s signal at 284.6 eV. The pressure during analysis was ca. 7×10^{-7} Pa.

2.4 Wettability assessment

A set of sessile drop experiments was carried out with a goniometer (Ramé-hart, model 500) on both laser treated and untreated titanium surfaces. Distilled water was used as test liquid. The contact angles of water on untreated and laser-treated surfaces were measured at room temperature conditions with a liquid volume of 3 µL. To ensure the reproducibility of results, the number of contact angle measurements was typically in the range of 6–10.

3 Results and discussion

3.1 XPS analysis of single-stage and dual-stage atmosphere controlled laser processing of titanium

Analysis of the laser-processed Ti surfaces was based on the previous literature that has looked at XPS of both titanium oxide and titanium nitride. The main studies used include XPS studies on the reduction of the native titanium oxide

TiO_2 to Ti_2O_3 and TiO via ion beam sputtering [22, 23], a detailed XPS study of titanium and its oxides [24], XPS studies that investigates the oxidation of titanium nitride [25, 26], and an XPS study that looked at oxide-free titanium nitride growth via sputter deposition and reactive evaporation [27]. These previous studies give insight into the chemical nature that is occurring during the atmosphere-controlled laser processing of a titanium surface with a native oxide present. This laser process is unique, in that, previous works have investigated the oxidation of titanium nitride, but not the nitriding of titanium oxide. In particular, understanding whether the femtosecond laser process is forming a TiON complex—as seen in the oxidation of titanium nitride studies [25, 26]—or if the laser process is reducing the native oxide—similar to the ion beam studies on titanium oxide [22, 23]—and creating a separate, non-complex titanium nitride peak [27]. These works allow us to compile a table of expected peaks for both the $Ti2p_{3/2}$ and N1s regions, shown in Table 3.

With these previous results and works, the analysis approach for the XPS data of the laser processed titanium surfaces is going to be approached by splitting the two-stage controlled atmosphere laser process into single-stage Ar atmosphere and single stage N_2 atmosphere experiments to investigate the complex nature of both the native oxide restructuring under an Ar-controlled environment and the chemical incorporation of TiN under a N_2 environment. For the main regions investigated ($Ti2p_{3/2}$ and N1s), all fitted components are assumed to have very similar FWHMs. It is also important to note that the XPS was taken after the sample was exposed to atmosphere immediately following the laser processing. This means that there is a re-oxidation of the processed titanium surface and that the complete reduction or removal of the native oxide is not observable in this study.

3.1.1 XPS analysis of titanium reference sample with native oxide

To start the XPS analysis, a reference sample of titanium with a native oxide was first performed. This sample came from the same bulk piece of titanium as all laser-processed samples.

Looking at Fig. 3, the XPS from the reference sample shows a single, dominant peak for the $Ti2p_{3/2}$ scan at 457.9 eV, showing that TiO_2 is the only surface state for the titanium sample. In addition, the N1s scan shows a peak at 399.7 eV—likely a contaminant from atmosphere exposure—and no peak at the expected TiN peak at 397 eV. This shows that the titanium samples start with a stable TiO_2 surface oxide and no nitride formation, as expected.

Table 3 Expected chemical peaks for both the $Ti2p_{3/2}$ and N1s regions for both titanium oxide and oxidized titanium nitride

References	$Ti2p_{3/2}$ region						N1S region	
	TiO_2	Ti_2O_3	TiO	Intermediate	TiN	Ti	N^I	N^{II}
Carley et al. [24]	459.0 eV	457.5 eV	455.5 eV	N/A	N/A	453.9 eV	N/A	N/A
Saha et al. [25]	459.1 eV	N/A	N/A	457 eV	455.3 eV	N/A	395.7 eV	397.1 eV
Esaka et al. [26]	458.8 eV	N/A	N/A	457.1 eV	455.6 eV	N/A	396.6 eV	397.8 eV
Prieto and Kirby [27]	N/A	N/A	N/A	N/A	454.7 eV (sp), 455.1 eV (re)	N/A	N/A	397.1 eV (sp), 396.9 eV (re)

Measurements were taken in the presence of titanium oxide, and sp and re denote sputter deposition and reactive evaporation, respectively

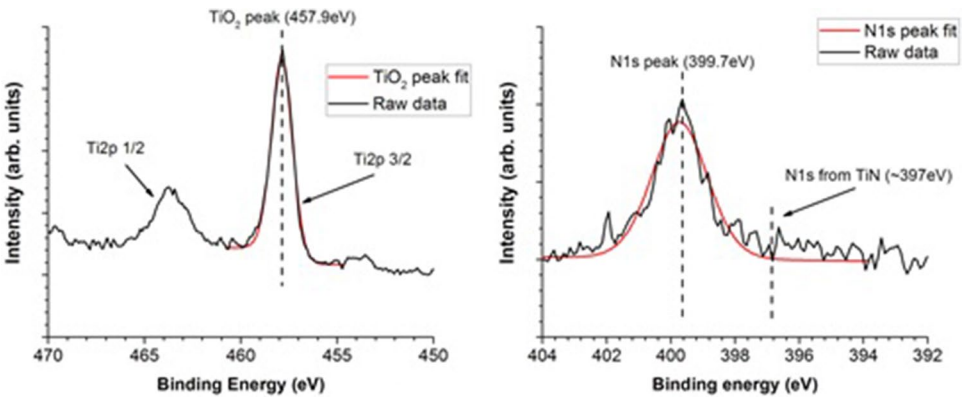

Fig. 3 Ti2p region (left) and N1s region (right) for an unprocessed reference titanium sample with native oxide

3.1.2 XPS of controlled Ar atmosphere single-stage laser-processed titanium surfaces

The Ar atmosphere stage is the first stage for the dual-stage laser process and is also a chemically inert environment for the titanium surface undergoing the laser processing. This means that any chemical changes seen in the XPS from these samples are due only to the interaction between the laser and the titanium surface, barring any interactions once the sample is re-exposed to atmosphere.

Figure 4 shows the XPS results from the femtosecond laser processing under controlled Ar atmospheres for both the Ti2p and N1s regions. The $Ti2p_{3/2}$ region shows the development of a small shoulder at lower binding energies from the TiO_2 peak location, centered at 458.5 eV. This shoulder consists of three different fitted peaks at positions of 456.8, 455.4, and 454.0 eV and, referring back to Table 3, correspond to Ti_2O_3, TiO, and metallic Ti, respectively. The presence of two additional oxide states than from the control XPS suggests that the laser process under Ar atmosphere partially restructures the native oxide and actually reduces the thickness of the oxide layer with metallic Ti now being observed, a process that is similar to that observed with ion bombardment of TiO_2. In addition, the binding energy of the TiO_2 peak has increased as compared to the control, and change of 0.6 eV, which is also observed during ion bombardment experiments [22, 23].

The N1s spectra show relatively small peaks for nitride formation at 396.4 eV. Given how small these peaks are, it is likely that the TiN contributions in the Ti2p spectra are simply hidden beyond the stronger TiO and metallic Ti fitted peaks. This does show that TiN forms in small quantities in the controlled Ar atmosphere experiments, likely once the laser processing is over and the sample has been reintroduced into air (and thus exposed to N_2). To compare the laser conditions used in the Ar atmosphere laser processing experiments, the compositions of TiO_2, Ti_2O_3, TiO, and metallic Ti are compared using the fitted peak areas in the $Ti2p_{3/2}$ region.

Figure 5 shows the composition of the restructured Ti oxides and the metallic Ti for the controlled Ar atmosphere experiments. The restructured oxide does not drastically change with the increased laser power, with the Ti_2O_3 composition unchanging and the TiO percentage only increasing from 2.7 to 3.1%. For the metallic Ti, there is a small increase with increasing laser power, going from 4.6 to 5.0%. This is an expected trend since an increase laser power under Ar atmosphere should remove more oxide.

3.1.3 XPS of controlled N_2 atmosphere single-stage femtosecond laser processed Ti surfaces

The N_2 atmosphere laser processing step is the second step used in the dual-stage process, and is also the chemically active environment meant to create TiN under laser processing. With the results seen in the Ar atmosphere laser processing, we also expect that the laser will restructure the native oxide, but that TiN formation will occur as well.

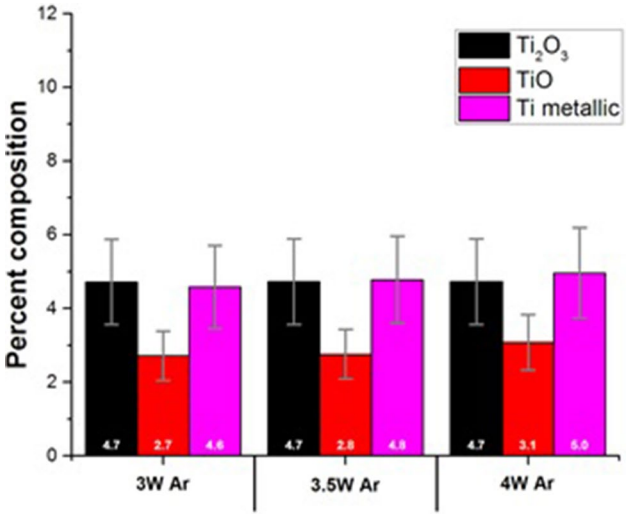

Fig. 5 Composition of the Ti samples processed under the controlled Ar atmosphere for Ti_2O_3, TiO and metallic Ti

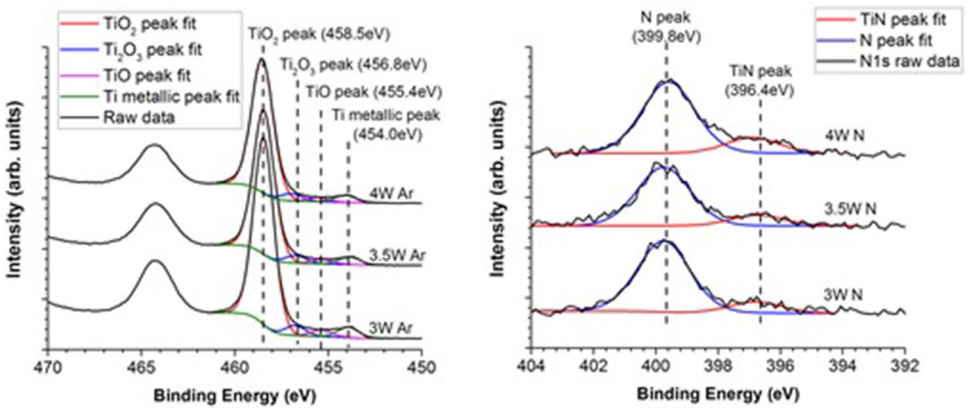

Fig. 4 Ti2p peaks (left) and N1s peaks (right) for the titanium samples processed under a controlled Ar atmosphere

The Ti2p spectra for controlled N_2 atmosphere experiments, shown in Fig. 6, initially seem very similar to the controlled Ar atmosphere experiments. The shoulders to the right of the $Ti2p_{3/2}$ TiO_2 peaks are quite small, but with the right most peaks centered at 454.7 eV instead of 454.0 eV as observed in the Ar experiments. Referring Table 3, it is found that the binding energy for this corresponds to the TiN XPS of the sputter grown film by Prieto and Kirby [27]. In fact, no metallic Ti is observed in any of the XPS spectra, located at 454.0 eV. The titanium oxide peaks are centered at 458.4, 457.0, and 455.9 eV for TiO_2, Ti_2O_3, and TiO, respectively. Even with the introduction of titanium nitride, the oxide peaks do not seem to be shifted significantly beyond the observed shift due to the restructuring of the oxide.

In the N1s XPS spectra, a significantly larger N1s nitride peak (centered at 396.4 eV) is observed as compared to the controlled Ar atmosphere experiments. This shows that TiN is formed during the controlled N_2 atmosphere laser experiments as opposed to after the laser treatment once exposed to air, as seen with the controlled Ar atmosphere experiments. There is also no satellite peak observed in the N1s spectra.

The composition of the restructured oxide components and nitride are shown in Fig. 7. Overall there seems to be more restructuring of the oxide as compared to the controlled Ar atmosphere experiments, with Ti_2O_3 composition ranging from 6.8 to 8.0% and TiO composition ranging from 3.5 to 4.4%. There is not a clear trend with the oxide component compositions against laser power. However, for the TiN composition, increasing laser power does increase the composition, starting at 2.1% for 3.5 W laser power and going to 3.2% for 5 W laser power.

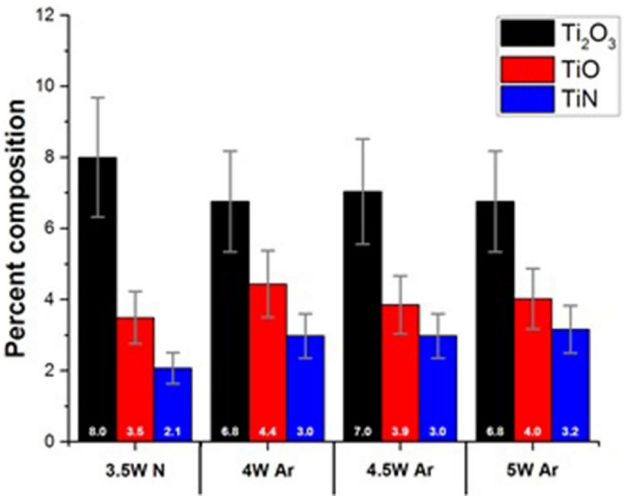

Fig. 7 Composition of the Ti samples processed under the controlled N_2 atmosphere for Ti_2O_3, TiO, and TiN

3.1.4 XPS of controlled atmosphere dual-stage femtosecond laser processed Ti surfaces

After going through the individual atmosphere-controlled laser processing steps, it is time to investigate the dual-stage laser process. The dual-stage process was created to remove and restructure the native oxide layer in the first Ar atmosphere step, as observed previously, and then follow-up with the N_2 atmosphere step to maximize titanium nitride formation.

Figure 8 shows the $Ti2p_{3/2}$ peaks for the 1_X titanium sample after the dual-stage femtosecond laser processing. Samples 2_X and 3_X had similar XPS results and analysis. Comparing the $Ti2p_{3/2}$ peaks to the single-stage cases, it is clear that the shoulder containing the Ti_2O_3, TiO, and TiN fitted peaks are significantly larger. This suggests that the amount of both oxide restructuring and nitride formation is increased in the two-stage process as opposed to the single-stage processes. The binding energies for the oxide components are at 458.4, 457.1, and 455.5 eV for TiO_2, Ti_2O_3, and TiO, respectively. These are very similar to the peak values observed in the N_2 single-stage laser process XPS results. The TiN peak has a binding energy of 454.7 eV, which is unchanged from the previous N_2 only experiment. This suggests that both the dual-stage and N_2

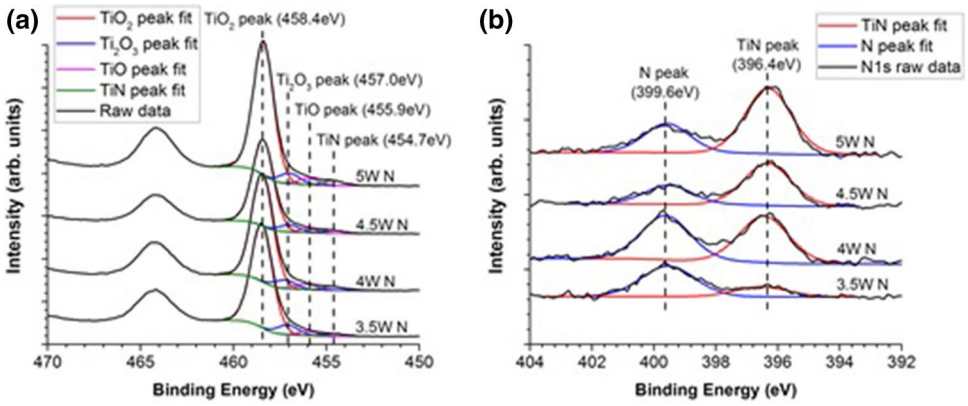

Fig. 6 Ti2p region (left) and N1s region (right) for the titanium samples processed under a controlled N_2 atmosphere

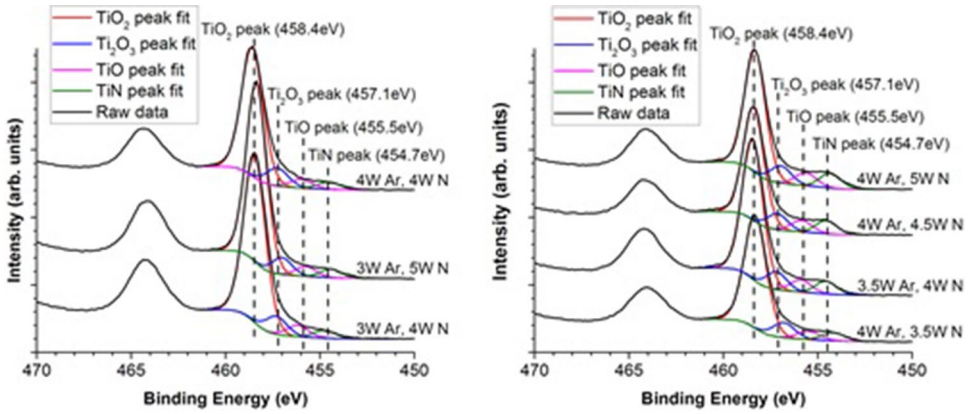

Fig. 8 Ti2p scans for the dual-stage controlled atmosphere experiments (Ar followed by N_2). Note that scans have an applied offset to visually compare them

only experiments produce TiN under the same mechanism, with no metallic Ti peaks present in the XPS spectra.

The N1s scans for sample 1_X, shown in Fig. 9, show the formation of a third peak at 398.3 eV, a peak that was not observed in the controlled Ar or N_2 atmosphere experiments. Looking back at Table 3, this third peak seems to have a significantly larger binding energy than the second N1s peaks observed in the oxidation of titanium nitride studies. Looking at the work done by Prieto and Kirby, they observed a satellite peak in the N1s region for the titanium nitride grown via the reactive evaporation method with a ΔB.E. of 1.7 eV from the main N1s peak [27]. Here, the third peak has a difference in binding energy of 1.8 eV which fits closer to the idea that the peak is a satellite peak of the nitride N1s peak. For the nitride N1s peak, the binding energy is 396.5 eV, very similar to the value seen in the single N_2 stage experiments. For the dual-stage experiments, the N1s nitride peak is also significantly larger for all 7 laser conditions. This shows that the dual-stage process is able to form a more significant titanium nitride composition than the single stage N_2 process.

The restructured oxide compositions and the nitride composition from all titanium samples subjected to the dual-stage laser process experiments, shown in Fig. 10, are typically larger than those from the single-stage laser process experiments. The largest nitride formation occurs with the 4 W/1.3 J cm^{-2} Ar, 5 W/1.6 J cm^{-2} N_2 laser conditions (referred 1_4 in Table 2), yielding a total TiN composition of 8.9%, with Ti_2O_3 and TiO at 10.4 and 7.8%, respectively. In terms of observed trends, more nitride formation is observed with higher laser cumulative power densities (until 4.5 W cm^{-2}) in both the Ar atmosphere and N_2 atmosphere stages, With increasing cumulative power density beyond 4.5 W cm^{-2}, percent of laser induced titanium nitride seems to decrease to reach 6.4 and 6.6% for titanium sample referred 3_1 and 3_2, respectively. Considering high values of repetition rate and number of pulse used at each stage of laser processing, the generation of localized plasma during the laser pulse above the titanium surface can be considered [28]. Beyond 4.5 W cm^{-2}, the plasma may reach high enough density to create a shielding effect harmful to the incorporation and nitrogen bonding to the titanium lattice.

Overall the XPS results show that titanium nitride can be formed on titanium with its native oxide under a N_2 environment with a femtosecond laser. In addition, performing a dual-stage process using an Ar-controlled atmosphere first followed by a N_2 atmosphere stage yielded nearly 3 times the nitride as compared to the single-stage N_2 atmosphere process. In regards to forming an oxynitride complex, specifically of the form N_x–Ti–O_y, there is no conclusive evidence

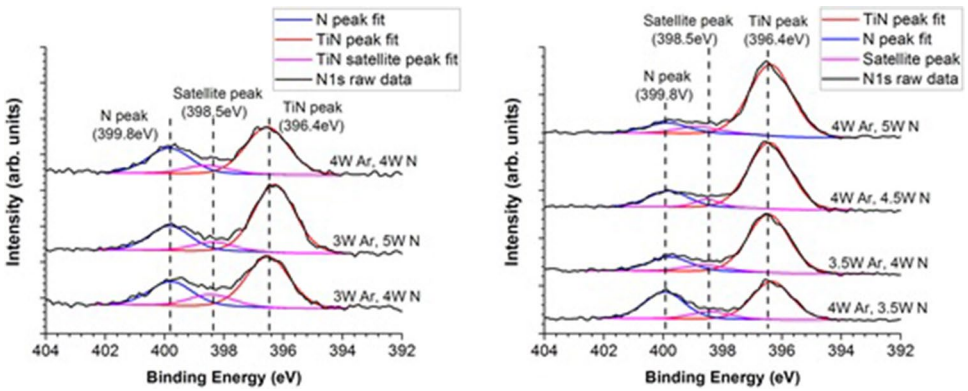

Fig. 9 N1s scans for the dual-stage controlled atmosphere experiments (Ar followed by N_2). Note that these scans have an applied offset to visually compare them

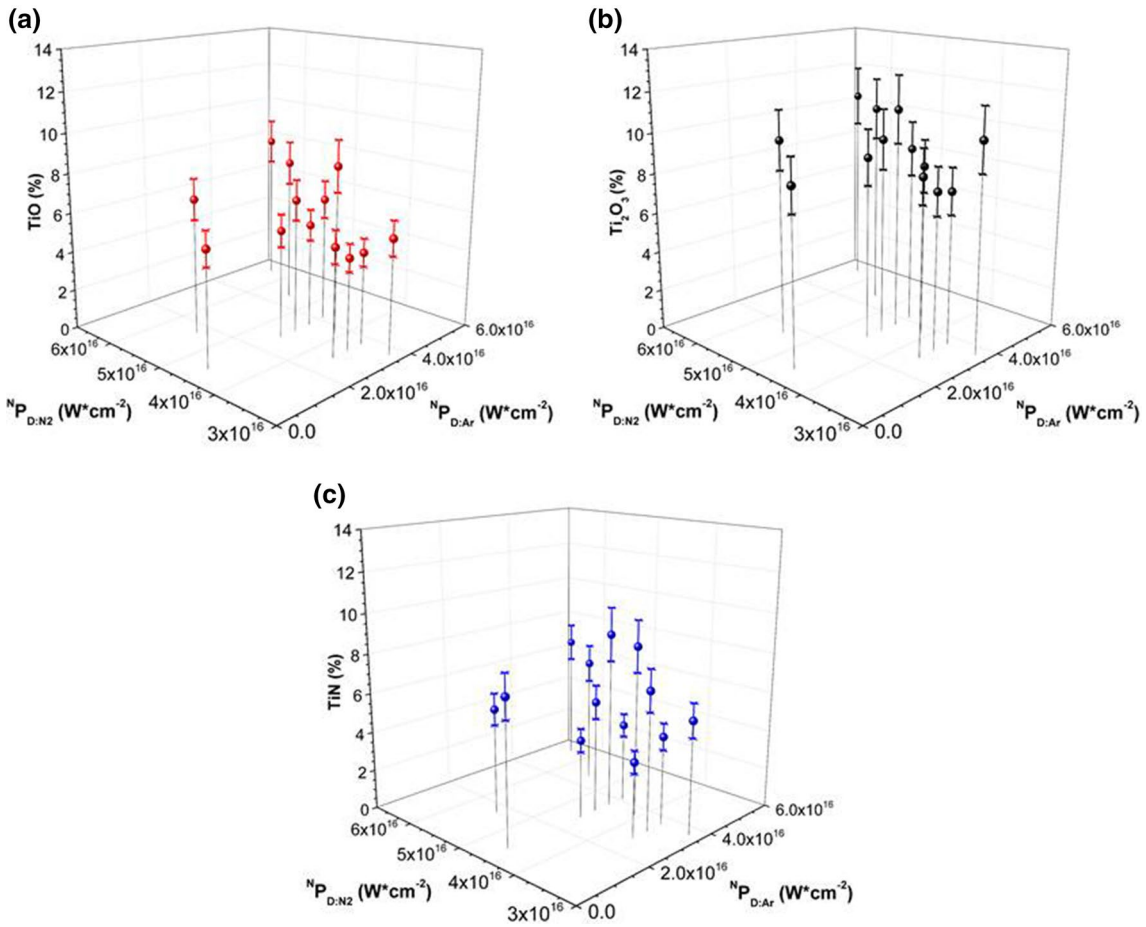

Fig. 10 3-D composition plots showing the composition of TiO (**a**), Ti_2O_3 (**b**), and TiN (**c**) with respect to the laser cumulative power densities from both the controlled Ar atmosphere and N_2 atmosphere stages

that one is formed during the controlled atmosphere laser process experiments. Unlike in the oxidation of titanium nitride experiments, the oxide components in the $Ti2p_{3/2}$ region are all fully quantifiable and have binding energies consistent with restructured TiO_2, and there is only a single nitride peak present in the N1s region as opposed to the two observed in the titanium nitride oxidation experiments [25, 26]. This suggests that the nitride formation occurs only with a "free" Ti atom and the restructured oxide does not react with any formed TiN. Likely any TiN formed at the very surface does oxidize.

3.2 Topographic characterization of surfaces process by laser in a reactive gas environment

3.2.1 Characterization of single-stage laser process induced surface morphologies

In the current investigation, femtosecond laser surface processing at high repetition rates of 1 MHz systematically induced topographic modifications of titanium surfaces. First, the results obtained from laser irradiation processed under either argon or nitrogen controlled environment (single-stage laser process experiment) are described. Figures 11 and 12 present SEM images of laser induced surface morphologies on titanium after irradiation under argon and nitrogen at different fluences, respectively. In both figures, SEM images clearly show the effect of the laser irradiation on the generation of self-organized multi-scale surface structures. Nevertheless, for approximately the same range of fluences (see Table 1), it seems that the gas environment strongly influenced the geometry of surface structures observed after laser irradiation. Figure 11a–c show laser induced surface morphologies under argon at 0.95 J cm^{-2} (3 W), 1.1 J cm^{-2} (3.5 W) and 1.3 J cm^{-2} (4 W). All of these images show microscale grooves covered by fuzz particles probably ejected from craters during laser ablation process. One can also notice that the grooves become significantly finer with increasing fluence. From approximately 2 µm width at 0.95 J cm^{-2}, width of mount-like structures between grooves decreases around 700 nm.

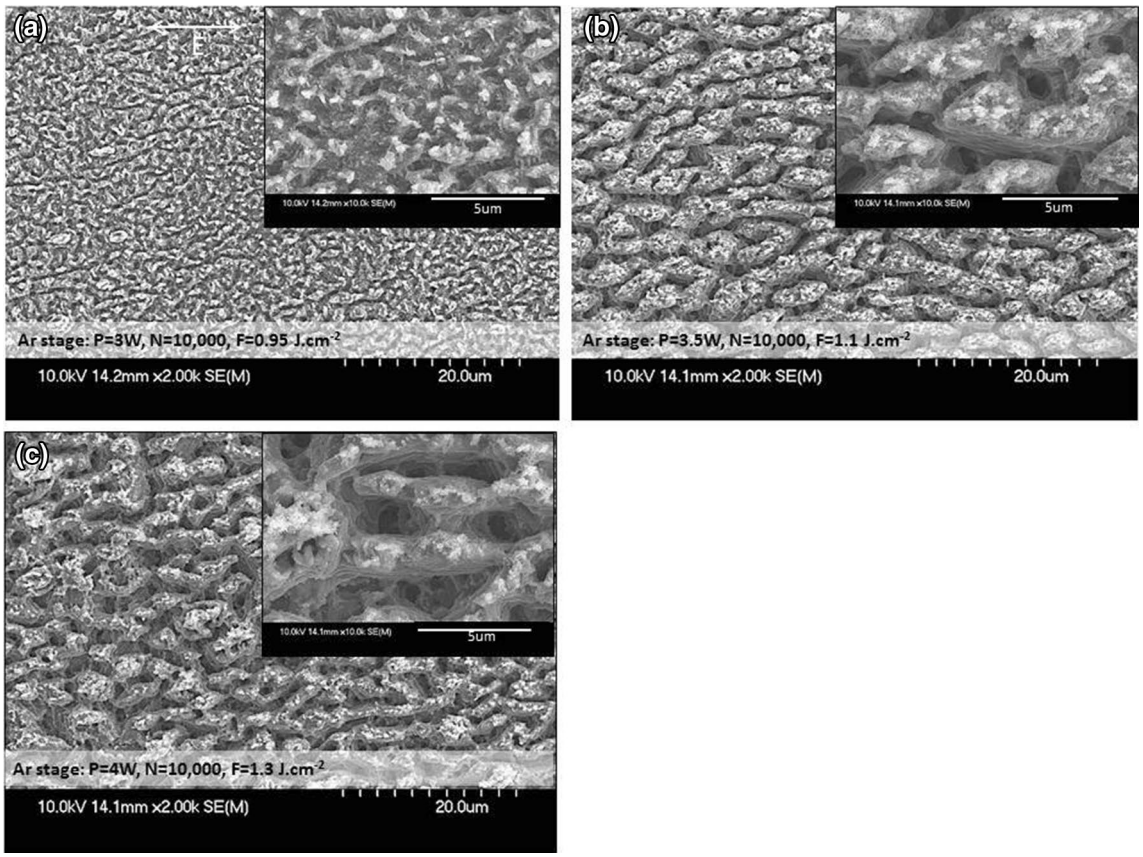

Fig. 11 SEM images of titanium sample referred 0_1_X (Table 1) processed by femtosecond laser under Ar atmosphere at **a** 0.95 J cm^{-2} (3 W), **b** 1.1 J cm^{-2} (3.5 W) and **c** 1.3 J cm^{-2} (4 W). Direction of laser polarization $\vec{E}$ during experiments is indicated by the arrow

Figure 12a–d show laser-induced surface morphologies under nitrogen at 1.1 J cm^{-2} (3.5 W), 1.3 J cm^{-2} (4 W), 1.4 J cm^{-2} (4.5 W) and 1.6 J cm^{-2} (5 W), respectively. Self-organized periodic nanostructures commonly called ripples or laser-induced periodic surface structures (LIPSS) are systematically observed on SEM images except on Fig. 12a at the lowest fluence tested 1.1 J cm^{-2}, where no surface morphologies were generated by laser irradiation (raw titanium surface). Ripples are one the observable phenomenon resulting from ultrashort laser–matter interaction (nano to femtosecond pulses) and already highly reported on a wide range of materials [8, 29]. In a certain energetic regime, irradiation with linear polarized laser involves the generation of surface structures aligned perpendicular or parallel to the incident electric field vector. From the literature, at least two types of ripples can occur from ultrashort laser interaction and have been categorized since. For normal incident radiation, Low Spatial Frequency LIPSS (LSFL) typically exhibit periods close to or slightly smaller than the irradiation wavelength ($\lambda/2 \leq \Lambda_{LSFL} \leq \lambda$), while High Spatial Frequency LIPSS (HSFL) have periods smaller than half of the irradiation wavelength ($\Lambda_{HSFL} < \lambda/2$). Current approaches towards understanding of the physical mechanisms of the LIPSS formation are based either on plasmonic or on hydrodynamic theories [30–34]. Beyond threshold fluence 1.1 J cm^{-2}, ripples are parallel to the direction of the laser polarization and cover titanium surface with a spatial periodicity around 213 ± 15 nm (example of AFM analysis on Fig. 13). The classical interpretation or model proposed to explain ripples phenomenology based on the interference between the incident laser light and excited surface plasmon wave, at normal incidence, predict ripples periodicity to approximate λ/n where λ is the wavelength of the incident light and n the refractive index of the irradiated material [35, 36]. Since the index of refraction of titanium at 1040 nm is 3.431, theoretical value of ripples periodicity is 301 nm and about 70% close to the experimental value, which could lead one to think that the interference interpretation could apply to ripples found in this study. Another topographic feature that one can notice is the presence of micro length cracks with increasing fluence. Although heat-affected zones (HAT) are limited when it comes to femtosecond laser surface processing, high repetition rate as well as the number of pulses per spot used in this study lead to heat accumulation and presence of cracks could result from the cooling phase post-irradiation [37].

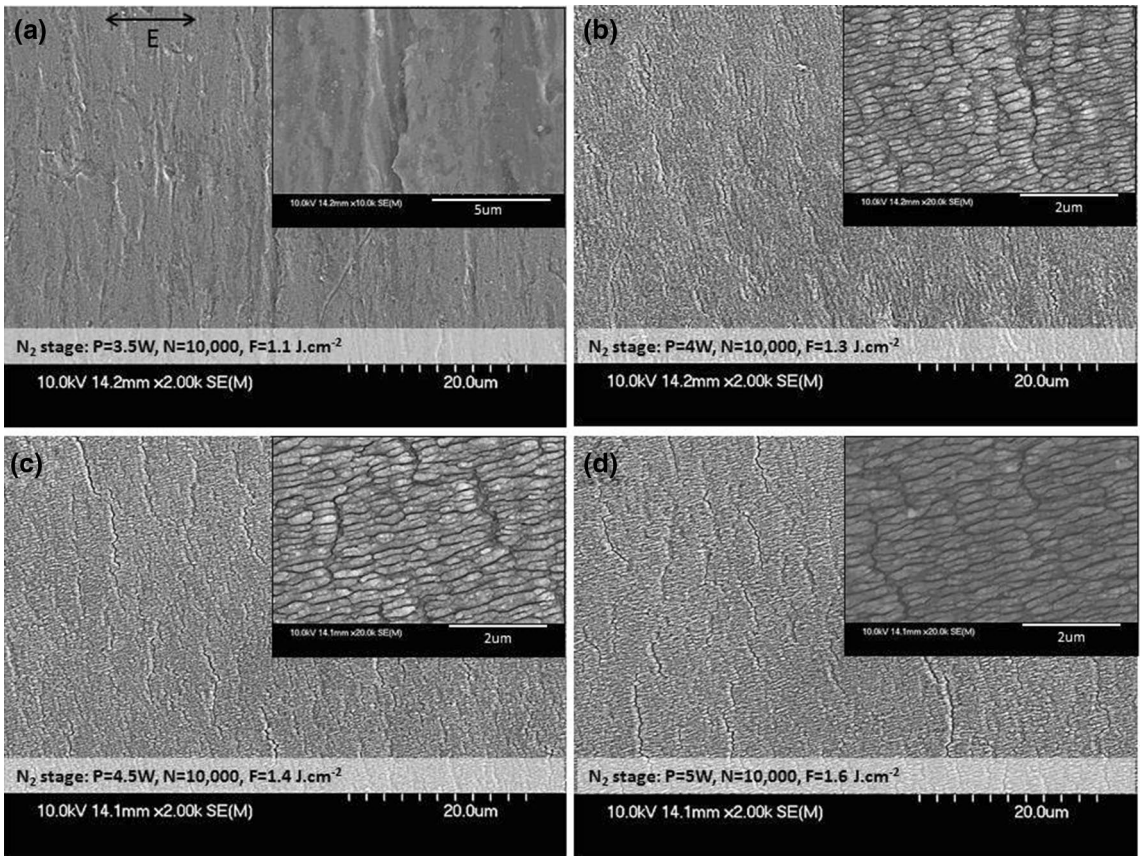

Fig. 12 SEM images of titanium sample referred 0_2_X (Table 1) processed by femtosecond laser under N_2 controlled atmosphere **a** at 1.1 J cm^{-2} (3.5 W), **b** 1.3 J cm^{-2} (4 W), **c** 1.3 J cm^{-2} (4.5 W) and 1.6 J cm^{-2} (5 W). Direction of laser polarization $\vec{E}$ during experiments is indicated by the arrow

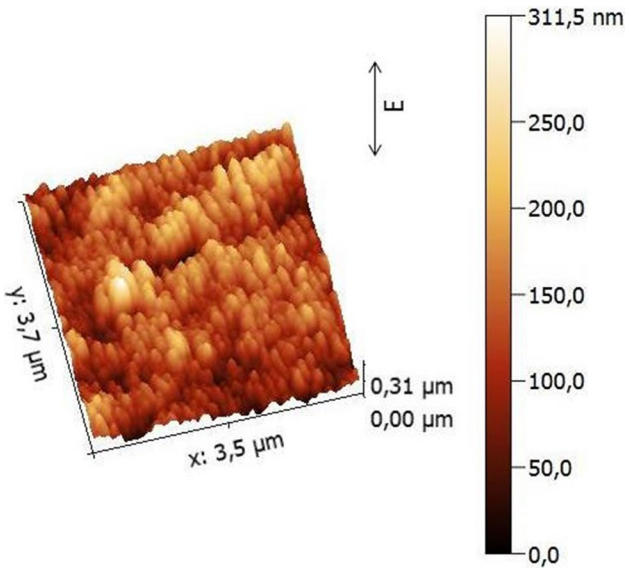

Fig. 13 AFM image of periodic ripples from titanium sample referred 0_2_1 (Table 1) processed by femtosecond laser under N_2 controlled atmosphere at 1.3 J cm^{-2} (4 W). To maximize lateral resolution, surface has been turned 90°

Laser-induced surface topography, as well as surface chemistry observed in an intense ultrashort regime depends not only on the type of target material but also with the gaseous medium the beam has to go through before to reach the target surface. Lehr [38] and Smausz [39] investigated the influence of the gas environment during the machining of micro-structures on titanium with a femtosecond laser and how it affects laser intensity efficiency and consequently both laser-induced surface chemistry and surface morphologies. Nayak et al. showed also that certain gas atmosphere could be chemically favorable to texture formation by ultrafast laser irradiation [40]. As demonstrated by Sun et al., nonlinear mechanisms can affect the refractive index of the gas environment in the vicinity of the laser pulses and then distorted the beam profile [41]. Sun et al. have identified two mechanisms responsible of medium's refractive index changes named Kerr effect and Plasma effect. In this study, the use of high pulse energies and high repetition rates could result in a strong ionization of the gas atmosphere at the gas–titanium interface. Plasma-induced effects such as beam distortion, defocusing or plasma shielding can occur and

could partially explain results observed regarding surface topography after laser irradiation.

3.2.2 Characterization of dual-stage laser process induced surfaces

Figures 14, 16 and 17 present SEM images of laser-induced surface morphologies results from two-stage experiments at different cumulative power densities on the titanium samples referred 1_X, 2_X and 3_X, respectively (see Table 2). From an overall point of view, variety of surface structures observed on these figures reflect the complexity of phenomena involved in the laser interaction process in a reactive gaseous medium. Two types of surface structures can be identified from Fig. 14 (sample referred to as 1_X) and present similitudes with the ones observed previously from single-stage experiments. First, SEM images, Fig. 14a, e, show ripples covering the surface and oriented parallel to the beam polarization. AFM analyses have been performed to assess spatial periodicity, shown in Fig. 15a, which was found to be around 212 ± 27 nm and particularly close to the value found for ripples generated under nitrogen-controlled atmosphere only (Fig. 12b–d). SEM images on Fig. 14b–d, f and g show surfaces covered by grooves with a clear reduction of fuzz particles on top of structures compared to morphologies previously observed after a single-stage laser process under argon controlled atmosphere (Fig. 11). AFM analysis has been performed on titanium surface exposed at 1.3 J cm^{-2} (4 W) as part of the dual-stage laser process as shown on Fig. 15b. It appears that height of surface structures approximates 3 µm which is significantly higher than ripples with an average height of 0.3 µm. With increasing fluence during the argon laser process stage (from 2.7 to 4.5 W cm^{-2}), morphologies under the form of protuberances seem to become larger and the overall microstructure appears coarser. It should be noted that fluence used during the N_2 step greatly influenced the resulting surface morphologies, namely fine ripples (Fig. 14a, e) and grooves patterns (Fig. 14b–d, f, g). In the case of fine ripples, fluence used during the N_2 step was significantly higher than fluence

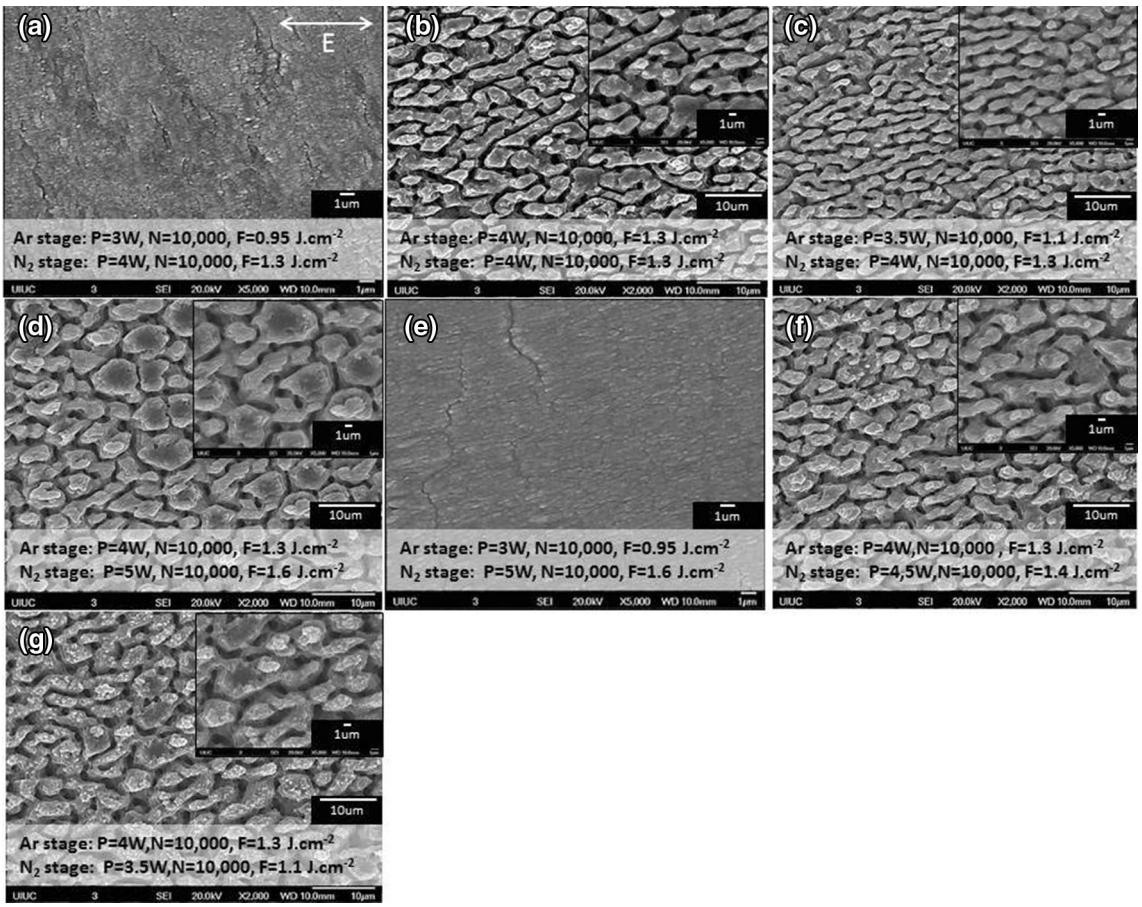

Fig. 14 SEM images of titanium sample referred 1_X (Table 2) subjected to dual-stage laser process at **a** Ar: 0.95 J cm^{-2} (3 W); N_2: 1.3 J cm^{-2} (4 W), **b** Ar: 1.3 J cm^{-2} (4 W); N_2: 1.3 J cm^{-2} (4 W), **c** Ar: 1.1 J cm^{-2} (3.5 W); N_2: 1.3 J cm^{-2} (4 W), **d** Ar: 1.3 J cm^{-2} (4 W); N_2: 1.6 J cm^{-2} (5 W), **e** Ar: 0.95 J cm^{-2} (3 W); N_2: 1.6 J cm^{-2} (5 W), **f** Ar: 1.3 J cm^{-2} (4 W); N_2: 1.4 J cm^{-2} (4.5 W) and **g** Ar: 1.3 J cm^{-2} (4 W); N_2: 1.1 J cm^{-2}(3.5 W). Direction of laser polarization $\vec{E}$ during experiments is indicated by the arrow

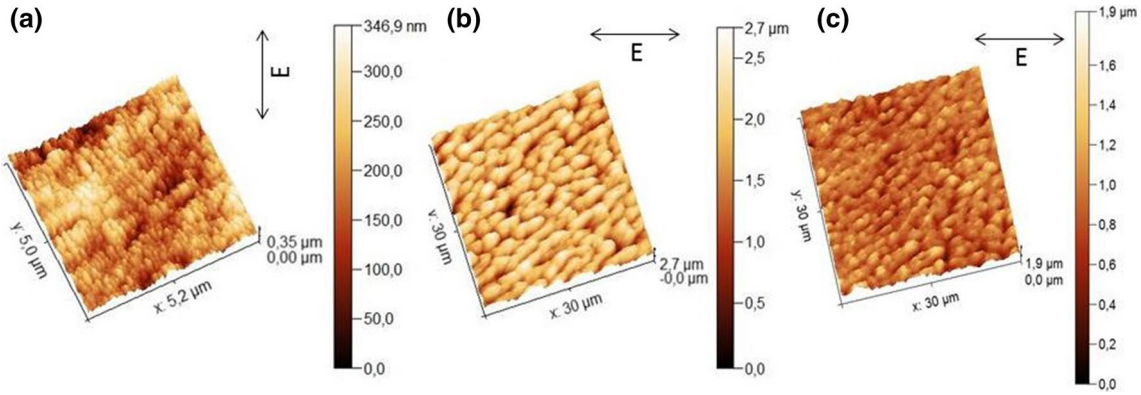

Fig. 15 AFM images of ripples and grooves found on titanium sample referred 1_1 and 1_2, respectively (Table 2), and subjected to dual-stage laser process at **a** Ar: 0.95 J cm^{-2} (3 W); N_2: 1.3 J cm^{-2} (4 W) (Fig. 14a), and **b** Ar: 1.3 J cm^{-2} (4 W); N_2: 1.3 J cm^{-2} (4 W) (Fig. 14b). AFM image of multiscale titanium surface (sample referred 2_2, Table 2) obtained through dual-stage laser process at Ar: 0.95 J cm^{-2} (3 W); N_2: 1.6 J cm^{-2} (5 W) (Fig. 16a). Fine ripples which overlapped on coarser protuberances composed this surface

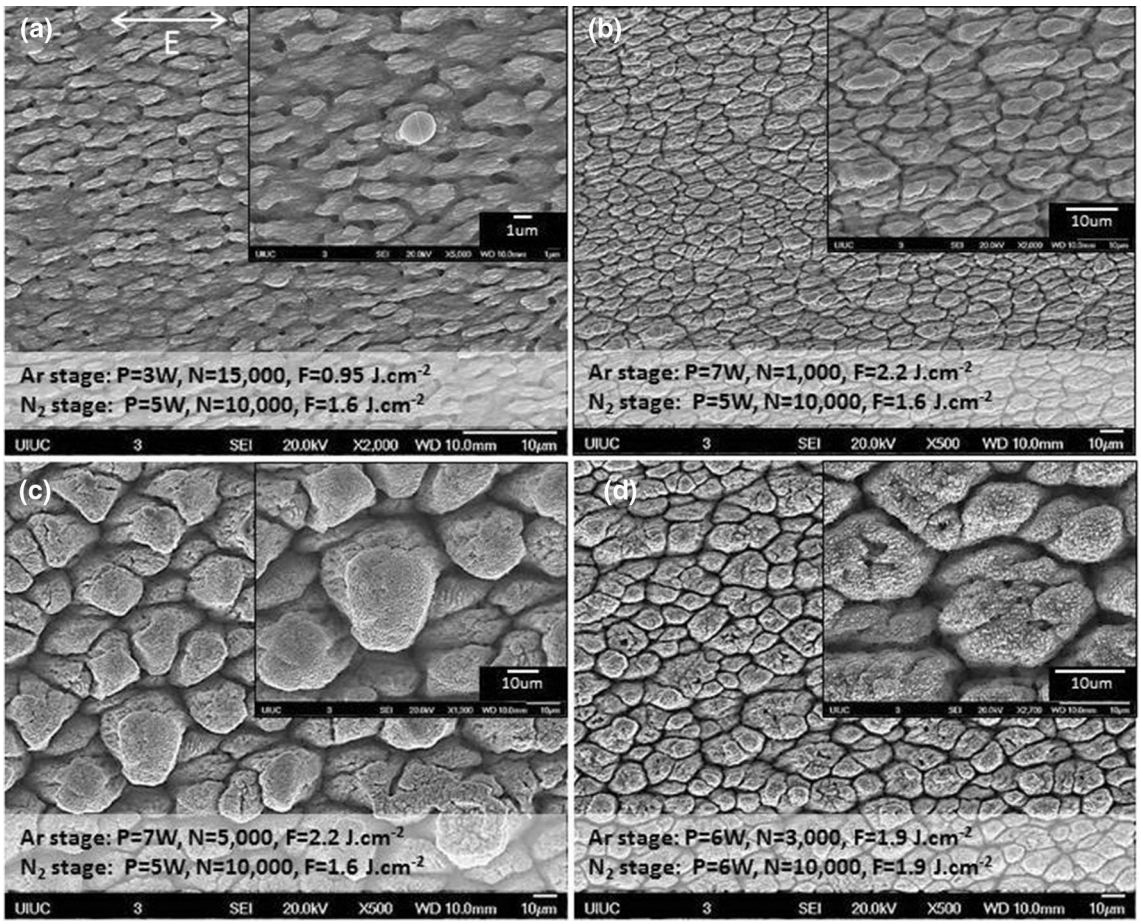

Fig. 16 SEM images of titanium sample referred 2_X (Table 2) subjected to dual-stage laser process at **a** Ar: 0.95 J cm^{-2} (3 W); N_2: 1.6 J cm^{-2} (5 W), **b** Ar: 2.2 J cm^{-2} (7 W); N_2: 1.6 J cm^{-2} (5 W), **c** Ar: 2.2 J cm^{-2} (7 W); N_2: 1.6 J cm^{-2} (5 W), **d** Ar: 1.9 J cm^{-2} (6 W); N_2: 1.9 J cm^{-2} (6 W). Direction of laser polarization $\vec{E}$ during experiments is indicated by the arrow

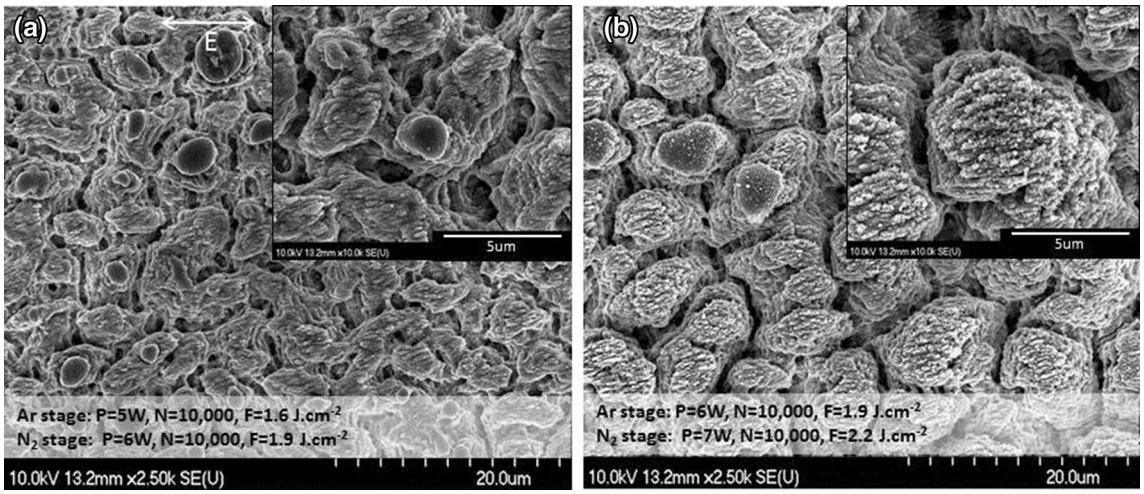

Fig. 17 SEM images of titanium sample referred 3_X (Table 2) subjected to dual-stage laser process at **a** Ar: 1.6 J cm^{-2} (5 W); N_2: 1.9 J cm^{-2} (6 W), **b** Ar: 1.9 J cm^{-2} (6 W); N_2: 2.2 J cm^{-2} (7 W). Direction of laser polarization $\vec{E}$ during experiments is indicated by the arrow

used during the Ar step, while grooves have been obtained using fluences similar or slightly higher during both Ar and N_2 steps (Table 2).

Figure 16 show SEM images of surface morphologies of titanium sample referred 2_X, irradiated at different fluences and number of pulses per spot (Table 2). Magnification of SEM images was not kept constant (from 2000 to 500) due to the evolution in scale of microstructures observed. SEM image on Fig. 16a shows a multi-scale surface with fine LIPSS which superimposed onto coarser protuberances which might appear as micro ripples. AFM analysis has been performed in the latter case, as shown on Fig. 15c. Microstructures on which ripples can be seen reach a height of 1.9 µm. SEM images on Fig. 16b–d show thoroughly different structures. Bumpy and pillow-like patterns are observed in these cases, with different density, shapes and diameters. One parameter which could explain the various surface features observed between Fig. 16a–d, independent of the applied fluence, is the number of pulses per spot used during the laser processing of titanium surface under argon controlled atmosphere. Morphologies observed on Fig. 16a have been created with a number of pulses per spot from 3 to 15 times higher than those used to generate structures shown Fig. 16b–d. If one compares laser parameters used to obtain groove patterns shown Fig. 14b–d, f and g and those used to induce the formation of bumpy and pillow-like structures shown Fig. 16b–d, fluences applied (regardless of the laser processing stage) are higher in the latter case. Moreover, cumulative power densities values which induce formation of bumpy and pillow-like structures (Fig. 16b, c) are also higher during the laser treatment stage under nitrogen controlled atmosphere.

Finally, Fig. 17a, b present SEM analyses performed on titanium sample referred 3_X. Cumulative power densities used to generate both type of surface structure shown on Fig. 17a, b (regardless of the laser processing stage) are the highest from Table 2. Moreover, independent of the number of pulses per spot which was kept constant at 10,000, fluences applied to form morphologies observed in Fig. 17b are higher to the one used to generate morphologies observed in Fig. 17a (regardless of the laser processing stage). The porous surface composed of islets of fine ripples which superimposed more chaotic and coarser protuberances shown in Fig. 16a evolve in surface composed of multi-scale bumpy structures which in turn exhibit fine ripples on their top with increasing fluence, as shown in Fig. 17b.

Ultimately, all laser conditions tested during dual-stage laser process experiments induced systematically hierarchical surface structures formation under the form of high-frequency periodic ripples, grooves, protuberances, bumpy or pillow-like patterns. It was demonstrated that the topographic functionalization of titanium surface by the generation of various morphologies, with different features in size and shape, is accessible by tuning both fluence and number of pulses per spot, at each step of the laser treatment, considering the plasma effects associated to each gaseous medium.

3.3 Water wettability assessment

XPS results as well as the topographic observations both show the high potential of titanium surfaces processed by dual-stage laser treatment for various applications. It was demonstrated that the largest nitride formation occurs with the 4 W/1.3 J cm^{-2} Ar and 5 W/1.6 J cm^{-2} N_2 laser conditions, yielding a total TiN composition of 8.9%. To compare the combined influence of surface chemistry and surface topography induced by a single-stage laser process or dual-stage laser process, water wettability have been assessed.

Table 4 Laser parameters used to create 1 cm^2 laser surface texturing on titanium samples referred as 4_X, for water contact angles measurements

Ref. sample	Gas environment	N	P (W)	F (J cm^{-2})	$^{N}P_{D}$ (W cm^{-2})	Contact angle (°)
Untreated Ti						93 ± 0.5
4_1	Argon	10,000	3	0.95	2.7E+16	51 ± 3.4
4_2	Argon	10,000	4	1.3	3.6E+16	54 ± 0.6
4_3	Nitrogen	10,000	4	1.3	3.6E+16	51 ± 2.2
4_5	Nitrogen	10,000	5	1.6	4.5E+16	41 ± 1.4
4_6	Argon	10,000	4	1.3	3.6E+16	35 ± 2.5
	Nitrogen	10,000	5	1.6	4.5E+16	

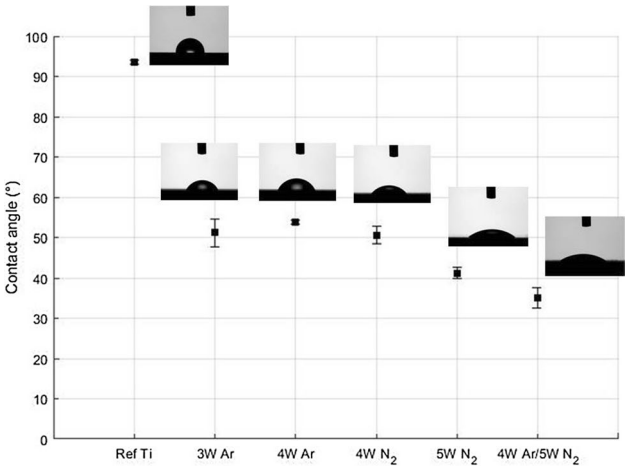

Fig. 18 Evolution of water contact angle assessed on untreated and laser treated titanium, as a function of both laser processing power and gaseous medium used (number of pulses was kept constant at 10,000)

1 cm^2 laser surface texturing were performed on titanium samples (Fig. 2b), according to laser parameters and gas conditions detailed in Table 4.

Figure 18 shows the evolution of water contact angle assessed on untreated and laser-treated titanium, as a function of both laser processing power and gaseous medium used (number of pulses was kept constant at 10,000). One can observe from Fig. 18 that the water contact angles of all laser-treated surfaces, regardless the type of process applied, are lower than 90°, indicating their transition from hydrophobic to hydrophilic after laser irradiation. Contact angle decreases from 93° ± 0.5° for the untreated titanium, to reach 35° ± 2.5° for the sample with the highest TiN composition (4 W/1.3 J cm^{-2} Ar and 5 W/1.6 J cm^{-2} N_2), a difference of 58°. Contact angles measured on titanium processed only under argon or nitrogen-controlled atmosphere show also drastic increase of treated surfaces wettability. First, the increase in surface wettability is attributed to both oxide reduction and their reconstructing resulted from laser surface processing under argon atmosphere, as shown by previous XPS analyses. Indeed, the interface between solid oxides and water exhibits an electromechanical double layer that generally prevents high wettability [42]. Second, the formation of hard phases such as Ti_2O_3, TiO rutile, and especially TiN during the laser surface processing under nitrogen atmosphere increases the surface strengthening and consequently the surface energy [43]. Hierarchical structures which combine multiscale morphologies (ripples, grooves), as shown by previous topographic analyses, generally enhance the phobicity of a surface [44, 45], which indicates in this case the strong influence of laser-induced chemistry changes on contact angles measurements.

4 Conclusion

There are a wide variety of applications when it comes to fs-laser processing of materials. One of the main applications of fs lasers is surface functionalization through both topography and chemistry modifications. In this paper, the influence of gas atmosphere and laser parameters on the formation of TiN by means of a dual-stage laser process is explored. Extensive XPS analysis has been performed to quantify laser induced surface chemistry after both single-stage and dual-stage laser process. The Ar-controlled atmosphere laser processing stage is the first step in the dual-stage process. It was demonstrated that the single stage Ar atmosphere laser processing partially restructures the oxide from TiO_2 to TiO and Ti_2O_3 (with TiO_2 still being the dominant oxide chemical state). This process also reduces the overall oxide thickness, as seen with the metallic peak observed at 454.0 eV. General trend is that the higher the laser power, the more partial oxide restructuring occurs and Ti metallic peak exposed. The N_2 atmosphere laser processing step is the second step used in the dual-stage process. It was shown that the single stage N_2 atmosphere laser processing also partially restructures the oxide from TiO_2 to TiO and Ti_2O_3 (with TiO_2 still being the dominant oxide chemical state). However, instead of exposing the underlying Ti, the N_2 process creates a TiN bond seen at 454.7 eV ($Ti2p_{3/2}$ scan) and 396.4 eV (N1s scan). Percent TiN varies very little with increasing laser power/fluence, being between 2.1–3.2%. General trend is that the higher the laser power, the more partial oxide restructuring occurs and TiN formed. Finally,

the dual stage Ar and N_2 atmosphere laser processing shows a stronger partial restructuring of the oxide from TiO_2 to TiO and Ti_2O_3 (still with TiO_2 being the dominant chemical state). In addition, the dual stage process shows a stronger formation of TiN (same peaks observed in the N_2 case, just larger), ranging significantly depending on laser conditions from 3.8 to 8.9%. The general trend here is quite complicated since there are two independent laser steps. Highest nitride formation occurs with the larger Ar and larger N_2 laser fluences (typically), with an exception for lower Ar laser fluence and higher N_2 laser fluence. Nevertheless, TiN formation seems to be highly correlated to the oxide restructuring.

Characterization of both single-stage and dual-stage laser process induced surface morphologies has been performed as well. Both gas medium and laser parameters used in this study resulted in a wide variety of surface structures. From approximately the same range of laser fluence (0.95–1.6 J cm^{-2}), laser irradiation under Ar controlled atmosphere induced porous surfaces while laser irradiation under N_2 induced self-organized periodic structures or ripples, with a spatial periodicity around 213 nm. Differences observed in morphologies generated after single-stage laser process experiments could originate from the plasma-effect involved at the gas–surface interface. Dual-stage laser process experiments also induced hierarchical surface structures formation under the form of high frequency ripples (212 nm spatial periodicity), grooves, protuberances or pillow-like patterns. It was demonstrated that the topographic functionalization of titanium is accessible by tuning both fluence and number of pulses per spot considering the plasma effect associated to each gas atmosphere. Finally, water wettability was assessed by means of contact angle measurements on untreated titanium surface, and titanium surfaces resulting from either single-stage laser process or dual-stage laser process. From an initial hydrophobic state (93°), titanium transitioned to a hydrophilic state (41°–54°) after a single-stage laser process (regardless the gas atmosphere). Titanium subjected to a dual-stage laser process exhibits the lowest contact angle measured in this study (35°). Formation of Ti_2O_3, TiO and especially TiN, would lead to an increase in surface energy and consequently in an increase in wettability. Application of a dual-stage laser process on titanium surface revealed its high potential in terms of both chemical and topographic surface functionalization with generation of hydrophilic hierarchical surfaces composed of titanium nitride and titanium sub-oxides. Hydrophilic surfaces are favorable for the adhesion, which path the way for many applications.

Acknowledgements This work was supported by the DOE Phase II SBIR/STTR (award number DE-SC0011851) and Starfire Industries LLC. Parts of this research were carried out in the Frederick Seitz Materials Research Laboratory Central Facilities, University of Illinois, which is partially supported by the U.S. Department of Energy under Grant nos. DEFG02-07ER46453 and DE-FG02-07ER46471.

References

1. A.Y. Vorobyev, C. Guo, Multifunctional surfaces produced by femtosecond laser pulses. J. Appl. Phys. **117**, 033103:1–5 (2015)
2. A.Y. Vorobyev, C. Guo, Direct femtosecond laser surface nano/microstructuring and its applications. Laser Photonics Rev **7**, 3 (2013)
3. J. Bonse, S.V. Kirner, S. Höhm, N. Epperlein, D. Spaltmann, A. Rosenfeld, J. Krüger, Applications of laser-induced periodic surface structures (LIPSS), Invited Paper Proc. of SPIE Vol. 10092
4. S. Hammouti, B. Holybee, M. Christenson, M. Szott, K. Kalathiparambil, S. Stemmley, B. Jurczyk, D.N. Ruzic, Wetting of liquid lithium on microtextured fusion-relevant materials by femtosecond exposure. J. Nucl. Mat. **(Manuscript submitted for publication)**
5. C. Yao, S. Xu, Y. Ye, Y. Jiang, R. Ding, W. Gao, X. Yuan, The influence of femtosecond laser repetition rates and pulse numbers on the formation of micro/nano structures on stainless steel. J. Alloys Compd. **722**, 235–241 (2017)
6. N. Yasumaru, K. Miyazaki, J. Kiuchi, Fluence dependence of femtosecond-laser-induced nanostructure formed on TiN and CrN. Appl. Phys. A **81**, 933–937 (2005)
7. O. Armbruster, A. Naghilou, M. Kitzler, W. Kautek, Spot size and pulse number dependence of femtosecond laser ablation thresholds of silicon and stainless steel. Appl. Surf. Sci. **396**, 1736–1740 (2017)
8. J. Bonse, J. Krüger, S. Höhm, A. Rosenfeld, Femtosecond laser-induced periodic surface structures. J. Laser Appl. Vol. **24**, 4 (2002)
9. B.K.K. Nayak, M.C.C. Gupta, Self-organized micro/nano structures in metal surfaces by ultrafast laser irradiation. Optics and Lasers Eng. **48**, 940–949 (2010)
10. A. Vorobyev, C. Guo, Femtosecond laser structuring of titanium implants. Appl. Surf. Sci. **253**, 7272–7280 (2007)
11. S. Hammouti, A. Pascale-Hamri, N. Faure, B. Beaugiraud, M. Guibert, C. Mauclair, S. Benayoun, S. Valette, Wear rate control of peek surfaces modified by femtosecond laser. Appl. Surf. Sci. **357**, 1541–1551 (2015)
12. J. Bonse, S.V. Kirner, R. Koter, S. Pentzien, D. Spaltmann, J. Krüger, Femtosecond laser-induced periodic surface structures on titanium nitride coatings for tribological applications. Appl. Surf. Sci. **418**(Part B), 572–579 (2017)
13. N. Epperlein, F. Menzel, K. Schwibber, R. Koter, J. Bonse, J. Sameith, J. Krüger, J. Toepel, Influence of femtosecond laser produced nanostructures on biofilm growth on steel. Appl. Surf. Sci **418**, 420–424 (2017)
14. D. Hoeche, P. Schaaf, Laser nitriding: Investigations on the model system TiN. A review. Heat Mass Transf **47**(5), 519–540 (2010)
15. P. Schaaf, T.M. Kahle, E. Carpene, Reactive laser plasma coating formation. Surf. Coat. Technol. **200**, 608–611 (2005)
16. E. Carpene, M. Shinn, P. Schaaf, Free-electron laser surface processing of titanium in nitrogen atmosphere. Appl. Surf. Sci. **247**, 307–312 (2005)
17. E. Carpene, P. Schaaf, M. Han, K. Lieb, M. Shinn, Reactive surface processing by irradiation with excimer laser, Nd: YAG laser, free electron laser and Ti: sapphire laser in nitrogen atmosphere. Appl. Surf. Sci. **186**, 195–199 (2002)
18. J. Krüger, W. Kautek, Ultrashort pulse laser interaction with dielectrics and polymers. Adv. Polym. Sci. **168**, 247–290 (2004)

19. J.M. Liu, Simple technique for measurements of pulsed Gaussian-beam spot sizes. Opt. Lett. **7**(5), 196–198 (1982)
20. V. Belaud, S. Valette, G. Stremsdoerfer, B. Beaugiraud, E. Audouard, S. Benayoun, Femtosecond laser ablation of polypropylene: a statistical approach of morphological data. Scanning **36**, 209–217 (2014)
21. D. Nečas, P. Klapetek, Gwyddion: an open-source software for SPM dataanalysis. Centr. Eur. J. Phys. 10(1), 181–188 (2012)
22. E. McCafferty, J.P. Wightman, An X-ray photoelectron spectroscopy sputter profile study of the native air-formed oxide film on titanium. Appl. Surf. Sci. **1431**, 92–100 (1999)
23. T. Choudhury, S.O. Saied, J.L. Sullivan, A.M. Abbot, Reduction of oxides of iron, cobalt, titanium and niobium by low-energy ion bombardment. J. Phys. D Appl. Phys. **22 8**, 1185 (1989)
24. A.F. Carley, P.R. Chalker, J.C. Rivierеand, M.W. Roberts, The identification and characterisation of mixed oxidation states at oxidised titanium surfaces by analysis of X-ray photoelectron spectra. J. Chem. Soc. Faraday Trans. 1 Phys. Chem. Condens. Phases **83**(2), 351–370 (1987)
25. N.C. Saha, H.G. Tompkins, Titanium nitride oxidation chemistry: An X-ray photoelectron spectroscopy study. J. Appl. Phys. **72**(7), 3072–3079 (1992)
26. F.F.K.S.H. Esaka, K. Furuya, H. Shimada, M. Imamura, N. Matsubayashi, H. Sato, T. Kikuchi, Comparison of surface oxidation of titanium nitride and chromium nitride films studied by X-ray absorption and photoelectron spectroscopy. J. Vac. Sci. Technol. A Vac. Surf. Films **15**(5), 2521–2528 (1997)
27. P. Prieto, R.E. Kirby, X-ray photoelectron spectroscopy study of the difference between reactively evaporated and direct sputter-deposited TiN films and their oxidation properties. J. Vac. Sci. Technol. A Vac. Surf. Films **13**(6), 2819–2826 (1995)
28. X.L. Mao, W.T. Chan, M.A. Shannon, R.E. Russo, Plasma shielding during picosecond laser sampling of solid materials by ablation in He versus Ar atmosphere. J. Appl. Phys. **74**, 4915–4922 (1993)
29. R. Buividas, M. Mikutis, S. Juodkazis, Surface and bulk structuring of materials by ripples with long and short laser pulses: recent advances. Prog. Quantum Electron. **38**, 119–156 (2014)
30. J. Bonse, A. Rosenfeld, J. Krüger, On the role of surface plasmon polaritons in the formation of laser-induced periodic surface structures upon irradiation of silicon by femtosecond laser pulses. J. Appl. Phys. **106**, 104910 (2009)
31. G.A. Martsinovskii, G.D. Shandybina, D.S. Smirnov, S.V. Zabotnov, L.A. Golovan, V.Yu.. Timoshenko, P.K. Kashkarov, Ultrashort excitations of surface polaritons and waveguide modes in semiconductors. Opt. Spectrosc **105**, 67–72 (2008)
32. J. Reif, F. Costache, M. Henyk, S.V. Pandelov, Ripples revisited: non-classical morphology at the bottom of femtosecond laser ablation craters in transparent dielectrics. Appl. Surf. Sci. **197–198**, 891–895. (2002)
33. A. Borowiec, H.K. Haugen, Subwavelength ripple formation on the surfaces of compound semiconductors irradiated with femtosecond laser pulses. Appl. Phys. Lett. **82**, 4462–4464 (2003)
34. D. Dufft, A. Rosenfeld, S.K. Das, R. Grunwald, J. Bonse, Femtosecond laser-induced periodic surface structures revisited: a comparative study on ZnO. J. Appl. Phys. **105** 034908 (2009). https://doi.org/10.1063/1.3074106
35. J.E. Sipe, J.F. Young, J.S. Preston, H.M. van Driel, Laser-induced periodic surface structure. I. Theory. Phys. Rev. B: Condens. Matter **27**, 1141–1154 (1983)
36. J.F. Young, J.S. Preston, H.M. van Driel, J.E. Sipe, Laser-induced periodic surface structure. II. Experiments on Ge, Si, Al, and brass. Phys. Rev. B Condens. Matter **27**(2), 1155–1172 (1983)
37. J. Schille, R. Ebert, U. Loeschner, P. Regenfuss, T. Suess, H. Exner, Micro structuring with highly repetitive ultrashort laser pulses, in *Proceedings of LPM 2008 (June)—The 9th international symposium on laser precision microfabrication*, Quebec, Canada
38. J. Lehr, F. de Marchi, L. Matus, J. MacLeod, F. Rosei, A.-M. Kietzig, The influence of the gas environment on morphology and chemical composition of surfaces micro-machined with a femtosecond laser. Appl. Surf. Sci. **320**, 455–465 (2014)
39. T. Smausz, T. Csizmadia, C. Tápai, J. Kopniczky, A. Oszkó, M. Ehrhardt, P. Lorenz, K. Zimmer, A. Prager, B. Hopp, Study on the effect of ambient gas on nanostructure formation on metal surfaces during femtosecond laser ablation for fabrication of low-reflective surfaces. Appl. Surf. Sci. **389**, 1113–1119 (2016)
40. B.K. Nayak, M.C. Gupta, K.W. Kolasinski, Formation of nano-textured conical microstructures in titanium metal surface by femtosecond laser irradiation. Appl. Phys. A Mater. Sci. Process. **90**, 399–402 (2008)
41. S. Ju, J.P. Longtin, Effects of a gas medium on ultrafast laser beam delivery and materials processing. J. Opt. Soc. Am. B Opt. Phys. **21**, 1081–1088 (2004)
42. P.G. de Gennes, Wetting: statics and dynamics. Rev. Mod. Phys. **57**, 827 (1985)
43. F.M. El-Hossary, N.Z. Negm, A.M. Abd El-Rahman, M. Raaif, A. A. Abd Elmula, Properties of titanium oxynitride prepared by RF plasma, ACES 5, 1–14 (2015)
44. P. Bizi-Bandoki, S. Benayoun, S. Valette, B. Beaugiraud, E. Audouard, Modifications of roughness and wettability properties of metals induced by femtosecond laser treatment. Appl. Surf. Sci. **257**, 5213–5218 (2011)
45. A.-M. Kietzig, S.G. Hatzikiriakos, P. Englezos, Patterned superhydrophobic metallic surfaces. Langmuir **25**(8), 4821–4827 (2009)